




Novel Landslide Susceptibility Mapping Based on Multi-criteria Decision-Making in Ouro Preto, Brazil

José Roberto Mantovani¹ · Guilherme Taitson Bueno² · Enner Alcântara^{1,3}  · Edward Park⁴ · Ana Paula Cunha^{3,5} · Luciana Londe^{3,5} · Klécia Massi^{1,3} · Jose A. Marengo^{3,5}

Accepted: 23 March 2023 / Published online: 5 April 2023
© The Author(s), under exclusive licence to Springer Nature Switzerland AG 2023

Abstract

Weather-related disasters have caused widespread deaths and economic losses in developing countries, including Brazil. Frequent floods and landslides in Brazil are mostly climatic driven, often aggravated by human activities and poor environmental planning. In this paper, we aimed to map and discuss the susceptibility to landslides in the urban area of Ouro Preto, Brazil, a municipality with colonial and world heritage houses. We used data on precipitation, soil types, geology, digital elevation model (DEM), and land use and land cover (LULC) of high spatial resolution (1 m). The location of landslides in the urban perimeter was provided by the Civil Defense of Ouro Preto, and these were validated by fieldwork. A novel mathematical model based on multi-criteria decision-making (MCDA) and the Analytic Hierarchy Process (AHP) was used to map the susceptible areas to landslides. Results show that areas most affected by strong landslides were low-density vegetation (high susceptibility) and rocky outcrops (very high susceptibility). The largest areas susceptible to landslides are urban land use areas. Particularly, landslides that occurred in February 2022 in the region were related to intense soil saturation. With an average monthly rainfall of 122.60 mm, the uneven relief and edaphoclimatic characteristics had caused percolation of the surface runoff, naturally triggering landslides. This study supports mitigation efforts by local governments and decision-makers.

Keywords Vulnerability · Natural hazards · Heritage sites · AHP

Introduction

The report by the World Meteorological Organization and the United Nations Office for Disaster Risk Reduction shows that climate change and extreme events have caused an increase in disasters over the last 50 years. Importantly, from 1970 to 2019, (i), natural hazards accounted for 50%

of all disasters, 45% of related deaths, and 74% of related economic losses; (ii) more than 11 thousand reported disasters have been attributed to weather events, with over 2 million deaths and US\$3.47 trillion in losses; (iii) more than 91% of deaths occurred in developing countries; and (iv) economic losses have increased sevenfold in the 50-year period, from an average of US\$49 million to a staggering US\$383 million a day globally. In Brazil, extreme events and natural hazards, predominantly floods and landslides (Tominaga et al. 2009), are mostly climatic driven though their consequences are usually aggravated by human activities, coupled with a poor environmental planning (IPCC, Climate Change 2022, Alcântara et al. 2023). Landslide is defined as a mass movement of material, under the influence of gravity, such as rock or debris, down a slope and can happen suddenly or slowly over a period. Heavy rainfall and changes to the material's strength through weathering and erosion of the base of a slope are external factors that can lead to a landslide (Skilodimou et al. 2018).

Landslides reported during the rainy season of 2021/2022 in southeast Brazil were mostly caused by the

✉ Enner Alcântara
enner.alcantara@unesp.br

¹ Institute of Science and Technology, São Paulo State University, São José Dos Campos, SP, Brazil

² Institute of Socio-Environmental Studies, Federal University of Goiás, Goiânia, Brazil

³ Graduate Program in Natural Disasters, São Paulo State University, São José Dos Campos, SP, Brazil

⁴ National Institute of Education, Earth Observatory of Singapore and Asian School of the Environment, Nanyang Technological University (NTU), Singapore, Singapore

⁵ National Center for Monitoring and Early Warning of Natural Disasters (CEMADEN), São José Dos Campos, SP, Brazil

pore water pressure in the soil which destabilizes slopes. At the beginning of the rainy season (typically in October), pores that have developed through evapotranspiration during the dry season are filled by the rainwater. After a prolonged period of rain, the infiltrated water seeks the saturated soil, exerting pressure on its particles (Fernandes and Amaral 1996). The imbalance between soil moisture and available pore water space causes slope instability and, consequently, landslides. Regions of Brazil with heavy rainfall and the extension of mountain massifs, thus, experience frequent landslides. Particularly, in the humid tropics where outcrops are relatively rare due to the high rates of weathering and/or bioturbations, gravity often exceeds its resistance force (Oliveira and Brito 1998), causing repeated landslides.

In addition, land use and land cover changes related to urbanization also contribute to landslide susceptibility (Shu et al. 2019), with vegetation playing an important role in landslide protection (e.g., Kalsnes and Capobianco 2022). In southeast Brazil, Atlantic Forest (tropical rainforest) and Cerrado (tropical savanna) are continuously suppressed to make way for agriculture and urban areas, making these hilly areas more vulnerable to landslides. Quevedo et al. (2023) provided an appraisal review about the land use and land cover as a conditioning factor in landslide susceptibility.

Mapping landslide susceptibility is important for early identification and mitigation of landslide hazards. However, it can be extremely complicated because the phenomena can be affected by many factors such as rainfall, human activity, lithology, and geological structure. According to Domínguez-Cuesta (2013), susceptibility can be defined as “the state of being susceptible or easily affected.” That is, susceptibility can be interpreted as a probability of disaster occurrence. Various qualitative and quantitative methods were proposed to map the susceptibility of landslide (Mersha and Meten 2020), including the most commonly used method—Analytic Hierarchy Process (AHP). AHP consists of 4 steps: (i) identify the decision, (ii) conduct pairwise comparisons, (iii) calculate the importance weight of each criterion, and (iv) identify the best option. Thomas et al. (2021) used AHP and frequency ratio (FR) to map landslide susceptibility zones in Idukki District, India. Bahrami et al. (2021) used AHP and fuzzy landslide susceptibility in Gilan, Iran. AHP is also applied to other phenomena, such as forest fire risk (Nikhil et al. 2021; Amrutha et al. 2022).

In this paper, we aimed to map the susceptibility to landslides in the urban area of Ouro Preto, Minas Gerais state, southeast Brazil. Ouro Preto is one of the most vulnerable cities to recurrent landslides in Brazil, resulting in significant human and economic losses. Furthermore, the municipality currently lacks an updated landslide susceptibility map. Recently, part of a mountain (Morro da Forca) near

the city center, slipped (on 9 am, January 13, 2022) and destroyed at least two colonial and world heritage houses. Reports indicated unstable slopes following a heavy rainfall, although conditions were dry at the point of landslide occurrence (<https://blogs.agu.org/landslideblog/2022/01/14/ouro-preto-1/>, last accessed on September 17, 2022). Thus, the results of this study contribute to occupation planning guidelines and balanced development process of Ouro Preto and other regions with similar geographical and climatic conditions.

Materials and Methods

Study Area

The municipality of Ouro Preto is in Serra do Espinhaço, the central region of the state of Minas Gerais in Brazil, in the Quadrilátero Ferrífero (an area with iron-rich soil). Urban area constitutes approximately 5786 ha. Its estimated population was around 74,000 in 2018. The “Quadrilátero Ferrífero” is considered one of the main regions for iron mining in Brazil and one of the largest mineral areas of the world (Carvalho Filho et al. 2010). Ouro Preto borders nine municipalities in Minas Gerais: Catas Altas da Noruega, Itaverava, Ouro Branco, and Congonhas to the south; Belo Vale and Moeda to the west; Mariana to the east; and Itabirito and Santa Bárbara to the north. The city’s average altitude is around 1225 m. It is located 100 km from the capital Belo Horizonte, with the MG-482 highway as the main access route (Fig. 1).

This region is located on the transition between Cerrado and Atlantic Forest biomes (IBGE 1991). Regarding geology and geomorphology, the region is among the “chapada” domain (plateau found in the Brazilian Highlands), covered by savannas and gallery forests to the north and the forested “Mar de Morros” domain to the south (a Brazilian morphoclimatic domain translated in English as “Sea of Hills” because of the similarity of its hills to the sea waves). Mar de Morros is formed by metamorphic rocks of the Minas Supergroup, Rio das Velhas Supergroup, and the Maquiné Group. It is also in the “Quadrilátero Ferrífero” region. The predominant relief domains are undulating hills and plateaus, with slopes ranging from 5 to 55%, including the river plain, hills, and steep hills. In the river plains, there are slopes of less than 3%, formed by flat terrain. The main soil types are Haplic Cambisol, Red-Yellow Latosol, and Litholic Neosol (Fig. 4f).

The regional climate is subhumid temperate, with an average annual rainfall of 1605 mm, which intensifies during the rainy season. December is the wettest month with 357 mm, followed by January with 315 mm (INMET). The temperature varies between 6 and 28 °C. The quarter from

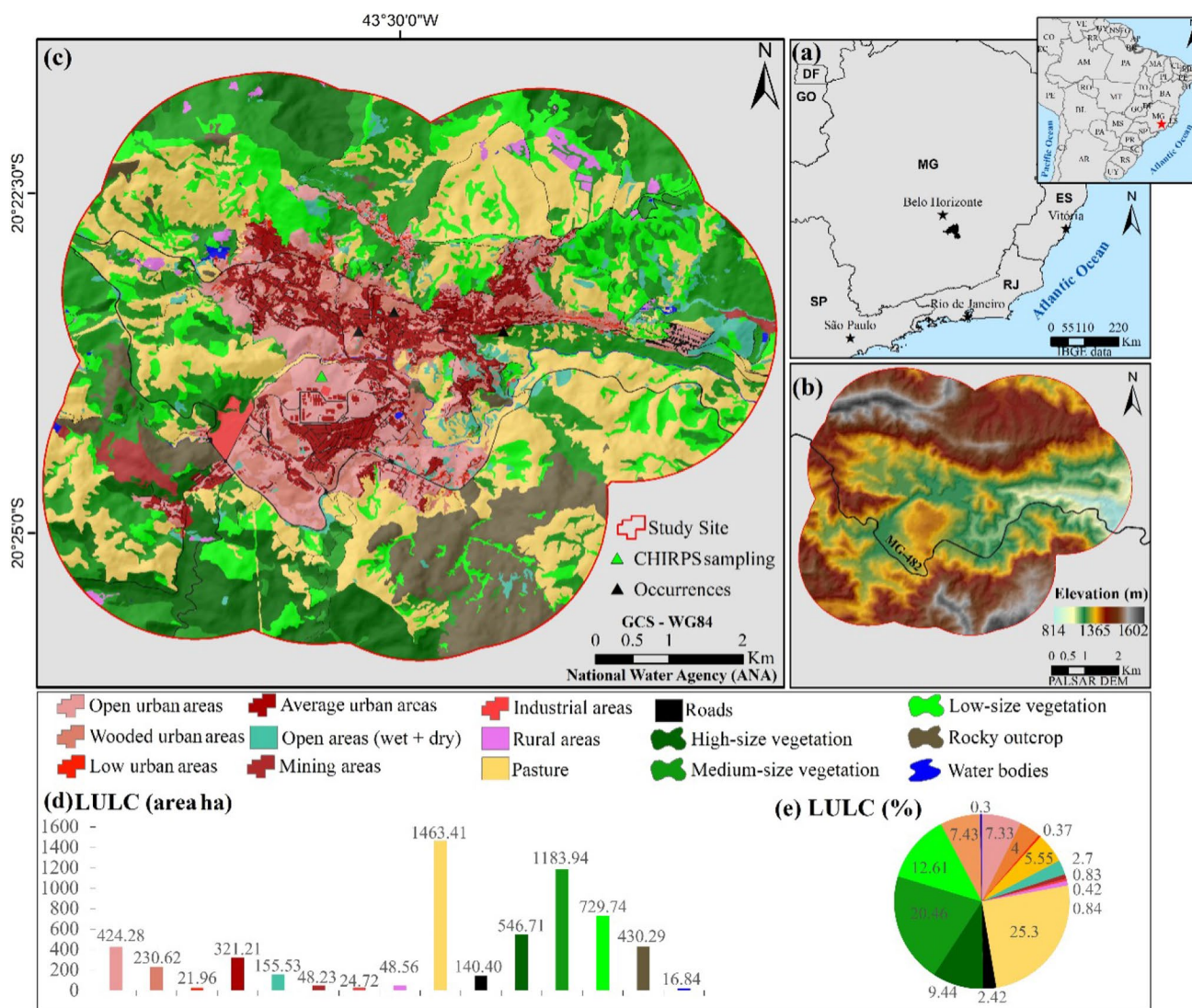


Fig. 1 a Location of the study site in Brazil; b the digital elevation model for the study area; c land use and land cover in the urban area of Ouro Preto (Minas Gerais state, Brazil) and CHIRPS sampling

spot used to extract the rainfall data from 1981 to February 2022 and the occurrences of the last event; (d) land use and land cover (LULC) area in hectare; (e) LULC in percent

December to February is characterized by the highest water surplus and the most active surface runoff. In January 2022, heavy rainfall of more than 200 mm in 24 h in some areas has caused further flooding and landslides in the state of Minas Gerais, Brazil, where at least 15 fatalities (<https://floodlist.com/america/brazil-floods-minas-gerais-january-2022>, last accessed on September 18 2022). Heavy rainfall was particularly severe in the state of Minas Gerais from 07 to January 11, 2022, corresponding to daily precipitation greater than 100 mm in the center of the state.

From 2003 to 2016, there were 52 decrees of public calamity and 2625 decrees of emergency in Minas Gerais, according to the official Brazilian website S2ID, ([https://s2id.mi.gov](https://s2id.mi.gov.br/paginas/series/)

[br/paginas/series/](https://s2id.mi.gov.br/paginas/series/)). During this period, there was one decree of emergency situation due to landslides in Ouro Preto, in December/2011 and January/2012. From 2017 onwards, the local civil defense started to publish received reports from citizens and other sources in their website, as follows (Table 1).

In December/2012, the main city hall and the municipality’s civil defense created the SAMOP—Ouro Preto’s Meteorological Warning System. This system is complementary to the local Contingency Plan for Disaster Risk Reduction and based upon technical works from the Federal University of Ouro Preto (UFOP). The SAMOP is aimed at warning the population and authorities about the possibility of landslide events, according to pluviometry thresholds.

Table 1 Details of floods and landslides published by the Ouro Preto's Civil Defense

Type of event	Date	Location
Flood	December 07th, 2017	Cachoeira do Campo
Flood	January 04th, 2018	Jardim Alvorada
Landslide	January 05th, 2018	Morro do Gambá
Flood	November 1st, 2018	Urban areas
Landslide	November 09th, 2018	Ladeira da Piedade
Landslide	November 23rd, 2018	Rua Padre Rolim
Landslide	December 03rd, 2018	BR 356
Flood	December 14th, 2019	Distrito de Santa Rita de Ouro Preto
Landslide	January 24th, 2020	Rua Dr Cláudio de Lima
Landslide	January 24th, 2020	Rua PADRE ROLIM
Landslide	January 24th, 2020	Rua Nossa Senhora dos Prazeres, no Morro da Queimada
Landslide	January 24th, 2020	Bairro Antônio Dias
Landslide	March 02nd, 2020	Road from Ouro Preto to Santa Rita
Landslide	March 02nd, 2020	Road from Ouro Preto to São Bartolomeu
Landslide	January 08th, 2022	Pandiá Calógeras
Flood	January 08th, 2022	Rua dos Esportes
Landslide	January 08th, 2022	Morro do Gambá
Landslide	January 08th, 2022	Rua Amarantina, Vila Aparecida
Landslide	January 09th, 2022	Bairro Piedade
Landslide	January 09th, 2022	Encosta Bairro São Francisco
Landslide	January 09th, 2022	Rua Osso de Boi, bairro Nossa Senhora do Carmo
Landslide	January 10th, 2022	Ladeira João de Paiva, morro São Sebastião
Flood	January 11th, 2022	Bairro Tavares
Landslide	January 11th, 2022	Condomínio Ze de duca morro Santana
Landslide	January 16th, 2022	Rua Santa Luzia
Landslide	February 23rd, 2022	Alameda da Olaria no bairro Nossa Senhora de Lourdes

Rainfall Dataset

Daily precipitation data were retrieved from the Climate Hazards Group Infrared Precipitation with Stations (CHIRPS) (Funk et al. 2015) from 1981 to 2022 and from MERGE (from 2001 to 2022), based on a technique for blending satellite and surface observations with 10-km spatial resolution (Rozante et al. 2010). Precipitation from weather stations of the National Center for Monitoring and Early Warning of Natural Disasters (CEMADEN) was also used for comparison purposes with satellite products since such stations do not have historical data.

Precipitation from CHIRPS was used to calculate the 5-day precipitation amount (R5day), and the daily precipitation from MERGE was used to estimate the maximum consecutive 5-day precipitation (RX5Max) and the critical precipitation coefficient (CPC, Castro 2006). The CPC is a numerical relation between the accumulated precipitation (PA) in 5 days and the daily precipitation (PD) associated with landslides. The following CPC equation (Eq. 1) was developed by Castro (2006) considering a precipitation time series from weather stations located in the municipality of Ouro Preto:

$$CPC = \frac{6386.6 \times PA^{-1.3847}}{PA} \quad (1)$$

According to Castro (2006), from the equation above, values of 5-day rainfall accumulation above 39.4 mm are equivalent to a CPC equal to 1.001, indicating a level of attention to landslides.

Landslide Susceptibility Mapping

The AHP multi-criteria decision-making method (Saaty 1977) via ArcGIS Pro was used to develop the methodology for landslide susceptibility mapping. The AHP method proposes to calculate the consistency ratio of judgments by estimating the random consistency index obtained for a reciprocal matrix of order n , with non-negative numbers and generated randomly (Bahrami et al. 2021; Leonardi et al. 2022).

Information on the types of soils (Fig. 4f), with a publication scale of 1:650.000 (EMBRAPA 2018), and geology, with a publication scale of 1:800.000 (CPRM 2006), were acquired from <https://bit.ly/3rkjbrD> and <https://bit.ly/geology-OP>, respectively. Data from the ANA (National Water

Agency) metadata catalog collection was used to characterize and map land use and land cover in high spatial resolution (1 m) of the urban area of municipalities. The mapping acquired information for the municipality of Ouro Preto, with a publication scale of 1:100.000, containing 15 classes (Fig. 1c).

The location of landslides in the urban perimeter was obtained in the image format on the civil defense portal of the municipality of Ouro Preto. The images were georeferenced, and each occurrence was vectorized manually. In total, 298 occurrences were mapped, obtained through modeling (CPRM), validated by fieldwork between 2012 and 2014, and updated by the Civil Defense of Ouro Preto until 2022.

The digital elevation model (DEM), scene AP_15549_FBS_F6770_RT1, uses Shuttle Radar Topography Mission (SRTM) data available on the website of Alaska Satellite Facility (ASF). They were resampled (upsampled) to 30 m for 12.5-m pixel size with orthometric altitude (EGM96 geoid model) and converted to geometrical altitude (ellipsoidal) from <https://search.asf.alaska.edu/#/>. A scene was also used from the thermal infrared sensor-2 (TIRS-2) and the Operational Land Imager (OLI-2), aboard the Landsat-9 Satellite, Level 2 (LC09_L1TP_218074_20220114_20220114_02_T1), with a resolution of 30 m, which was downloaded from the website of Earth Explorer (<https://earthexplorer.usgs.gov>).

Daily precipitation data from 1981 to 2021 were obtained from the Climate Hazards Group Infrared Precipitation with Stations (CHIRPS) (Funk et al. 2015). The precipitation data were analyzed using the box plot approach, and statistical analyses were applied to the time series to identify patterns and relationships between the variables of the data set for the application and calibration of the AHP model.

The precipitation time series was tested to identify its seasonality using the Augmented Dickey–Fuller (ADF) test and autocorrelation using the Durbin–Watson (DW) and Mann–Kendall tests. The last test is a robust, sequential, and non-parametric method used to determine whether a data series denotes a statistically significant time trend. The ADF test was used to verify the stability of the mean, standard deviation, and presence of seasonality (Fuller 1996). The null hypothesis states that if the time series has a unit root, it is not stationary. If seasonality is present in the time series, the data are not stationary. The DW test is widely used for autocorrelation in non-lagged dependent variables and when sample sizes are small. It varies from 0 to 4: values close to 2 (no autocorrelation); values close to 0 (positive autocorrelation); and values close to 4 (negative autocorrelation) (Durbin 1950, Durbin 1951). The null hypothesis is that there is no autocorrelation.

Trend analysis allows us to observe changes in behavior and determine which regions a particular variable has

undergone changes over time. The hypotheses adopted for the Mann–Kendall test are generally the following: H0 (null hypothesis): There is no trend present in the data; HA (alternative hypothesis): a trend is present in the data that can be either increasing or decreasing. The Theil-Sen Robust Linear Regression (TS) was used to confirm time-series trends (Sen 1968). Thiel-Sen is a median-based non-parametric estimation approach that makes no hypothesis about the distribution of the dataset and is insensitive to outliers. It returns the slope and intercept values with the ordinate axis, composing the classical regression line equation.

The results of the statistical analyses were used to calibrate the curve number (CN) model. The surface runoff generated in response to a given rainfall event is affected by the moisture content of the soil existing at the time when the rainfall begins. Thus, the precipitation accumulated on February 13, 2022, was used to estimate the approximate amount of surface runoff and the infiltration rate, determining the maximum water storage capacity of the soil after the start of the runoff.

Mapping and Analysis

Before applying the methodologies derived from the digital elevation model (DEM), the Fill Sinks algorithm was applied to fill the spurious depressions, assigning new values to the pixels with anomalies based on the information from the nearest neighbors (Wang and Liu 2006). The DEM was used throughout the research to map the relief dissection, apply the CN (curve number) method, calculate surface runoff and saturation, apply the topographic position index (TPI), and extract the slope of the study area. All variables obtained were examined in the pairwise comparison matrix using the AHP method.

The relief dissection map was obtained using the DEM of the SRTM sensor. The methodological procedures involved the steps described by Guimarães et al. (2017). The author emphasizes that to calculate the average interfluvial dimension, it is necessary to determine the threshold that defines the minimum drainage area for the delimitation of drainage basins (Medeiros et al. 2009). Thus, as proposed by Mantovani and Bueno (2021), a threshold of 1724 (count/pixel) was used to calculate the interfluvial dimension, executed through the conditional (con) function in the ArcGIS software.

The topographic position index (TPI) was also calculated using the DEM of the SRTM sensor, following the methodology proposed by Guisan et al. (1999) and using the SAGA-GIS software. The TPI-based relief classification uses a matrix that classifies the topographic position of each pixel with its altimetric relationship with neighboring pixels on two scales: large-neighborhood TPI and small-neighborhood TPI. The scales are

defined according to the nature of the phenomenon of interest. For broader scales, the TPI can be obtained from the elevation data, while for limited spatial scales, the TPI can be obtained from the slope data, according to the procedures described by Zimmerman (1998). Therefore, each relief class obtained combines information referring to the broader scale (elevation) and the local scale (slope). Thus, 10 relief classes were produced: high ridges, midslope ridges, local ridges, upper slopes, open slopes, plains, valleys, upland drainages, midslope Drainages, and Streams.

The soil moisture index (SMI) proposed by Zeng et al. (2004) is one of the most popular methods to estimate soil moisture with thermal remote sensing. It was used to obtain the indices of soil surface temperature and vegetation. The SMI is based on NDVI Normalized Difference Vegetation Index) and land surface temperature (LST) values between 0 (dry soil) and 1 (wet soil) (Zeng et al. 2004).

The methodological procedures described by Hassan et al. (2019) were used to obtain the SMI index. Pre-processing steps were applied to the satellite images to prepare them for calculating the LST and SMI. These steps can be divided into the following: atmospheric correction for thermal IR data; conversion of corrected thermal data (DN) to TOA spectral radiance; conversion of radiance (TOA) to effective sensor temperature; and conversion of corrected thermal IR data (DN) to emissivity. All these steps were calculated by importing the MTL correction parameters of the scene used.

Finally, the SMI was calculated by applying the maximum and minimum limits of the LST directly in Eq. 2, which was calculated using the ENVI 5.3 software.

$$SMI = \frac{LST_{\max} - LST}{LST_{\max} - LST_{\min}} \quad (2)$$

where SMI is the soil moisture index, LST is the land surface temperature, LST_{\max} is the maximum limit of retrieved LST, and LST_{\min} is the minimum limit of retrieved LST.

The SMI was calculated for the study area to reconstruct the soil moisture dynamics for the event that occurred on February 13, 2022, from the Landsat 9 satellite images dated January 14, 2022 (1 day after the movements in Ouro Preto-MG, Morro da Forca). The use of this date is justified because the area was covered by clouds on the day of the event. The SMI was used in the pairwise comparison matrix in the AHP method.

The modeling of surface runoff (Q) followed the theoretical and methodological procedures described by Mantovani et al. (2017), through the CN method, from the Soil Conservation Service, currently the Natural Resources Conservation Service (NRCS 2009). The CN method shows the effect of changes in land use and vegetation cover on surface runoff. The CN values range between 1 and 100 (dimensionless). High values of CN indicate high runoff (Melesse and Shih 2002).

In the CN method, the estimate of surface runoff (Q , mm) is calculated by Eq. 3.

$$Q = (P - 0.2) \times 2 \times P + 0.8 \times S \quad (3)$$

Here, P corresponds to the average monthly precipitation (mm/month), and S is the maximum water storage capacity (saturation) of the surface layer of the soil (Eq. 3).

Based on the analysis of the precipitation time series, the effective precipitation (P), which caused the surface runoff on February 13, 2022, was considered the monthly average precipitation value of 122.60 mm in February. To determine the maximum infiltration capacity of the surface layer of the land (S), the method relates this parameter to the CN factor, according to Eq. 4.

$$S = \frac{25400}{CN - 254} \quad (4)$$

where CN is the curve number and S is the maximum storage capacity of the soil (mm).

Equation 4 represents the soil cover conditions, ranging from a considerably permeable cover to a completely impermeable cover and from the soil with high infiltration capacity to one with low infiltration capacity. Thus, the CN values depend on land use and vegetation cover, types of soils reclassified into hydrological soil groups (HSG), and topographic characteristics, specifically slope, obtained through the DEM.

The general criteria proposed for elaborating the map of the HSG and the particularities of each class of soil present in the basin were defined according to the current Brazilian Soil Classification System (SiBCS) (EMBRAPA 2018). The system is based on the classification of Brazilian tropical soils proposed by Sartori et al. (2011). No type of soil was associated with hydrological group A (considered well-drained). The Red-Yellow Latosol was associated with hydrological group B. Further, there was no association with hydrological group C (considered moderately poorly drained). The Cambisol and Litholic Neosol were associated with hydrological group D as they presented poor drainage and susceptibility to erosive processes and landslides. Moreover, they are not thick (especially Litholic Neosol) and become saturated quickly.

The classification of thematic attributes of the land use and vegetation cover map was made. The processing was performed by joining the reclassified land use and vegetation cover maps and the HSG map through the HEC-Geospatial Hydrological Modeling Extension (GeoHMS) added to the terrain slope. After obtaining the CN grid through Eq. 4, we calculated the soil saturation rate (Eq. 5) as well as the soil saturation grid and the surface runoff used in the pairwise comparison matrix in the AHP method.

To validate the results, cross-tabulation graphs were prepared from the stratified classes of the mass movement map with the

mapped occurrences and classes of land use and vegetation cover (Fig. 1c). This was stratified into five classes: very low, low, moderate, high, and very high. A kernel density map was also generated to mark the occurrences of the landslides; the map was reclassified into five classes and stratified into densities: very low, low, moderate, high, and very high. Additionally, three occurrences were selected (Fig. 1a–c) with the respective photographs, one of them being the last event that occurred (January 13, 2022) in Morro da Forca.

Landslide Mapping Validation

The validation of AHP landslide mapping was done using a Boolean intersection approach (Shano et al. 2020). The interpretation of Boolean intersection is that nonzero values are considered true, and zero is considered false. We used the civil defense landslide mapping as a reference and the AHP model landslide result to apply the Boolean intersection. We excluded areas classified by AHP as having very small susceptibility to landslides to obtain the landslide occurrences in both data. The final Boolean map will show the correspondence between both data; therefore, we will be able to assess the potential and limitations of the AHP method in our study site.

Results

Analysis of the Precipitation Time Series

The average annual rainfall data (Fig. 2) from 1981 to 2021 was 125.20 mm, with a minimum and maximum of

2.75 and 540.62 mm, respectively. The heaviest rainfall occurred in 2008, and the lowest was in 2017. The heaviest average rainfall (170.80 mm) occurred in 1985. The heaviest and average rainfalls from January to February 2022 were 122.60 and 347.64 mm, respectively.

Considering only February 2022, the month when the analyzed event occurred, the average precipitation was close to that of the entire time series analyzed. Next, the statistical tests for the time series demonstrate the temporal variability of precipitation in the study area.

Figure 3a shows the 5-day rainfall from MERGE, corresponding to January 8–12, 2022, which recorded the highest 5-day accumulated rainfall in January (347 mm). It corresponds to weather station data from CEMADEN (344 mm) located in the study area. Considering the annual scale, this heavy rain event in 2022 was the fifth largest in the period 2001 to 2022 (Fig. 3c).

Figure 3b indicates that only in January 2022, 11 periods of 5-day rainfall accumulation were above 39.4 mm over the study area (threshold for landslides established by Castro 2006). The temporal evolution of the CPC considering the 5-day rainfall accumulation indicates an increasing pattern, mainly from pentad 8.

The results of the Dickey–Fuller test (Table 2) show that the calculated p -value is greater than the significance level $\alpha=0.05$. Therefore, the null hypothesis cannot be rejected—the precipitation time series is not stationary. The risk of rejecting the null hypothesis when it is true is 28.52%. Therefore, the statistical properties of the precipitation time series are changing over time.

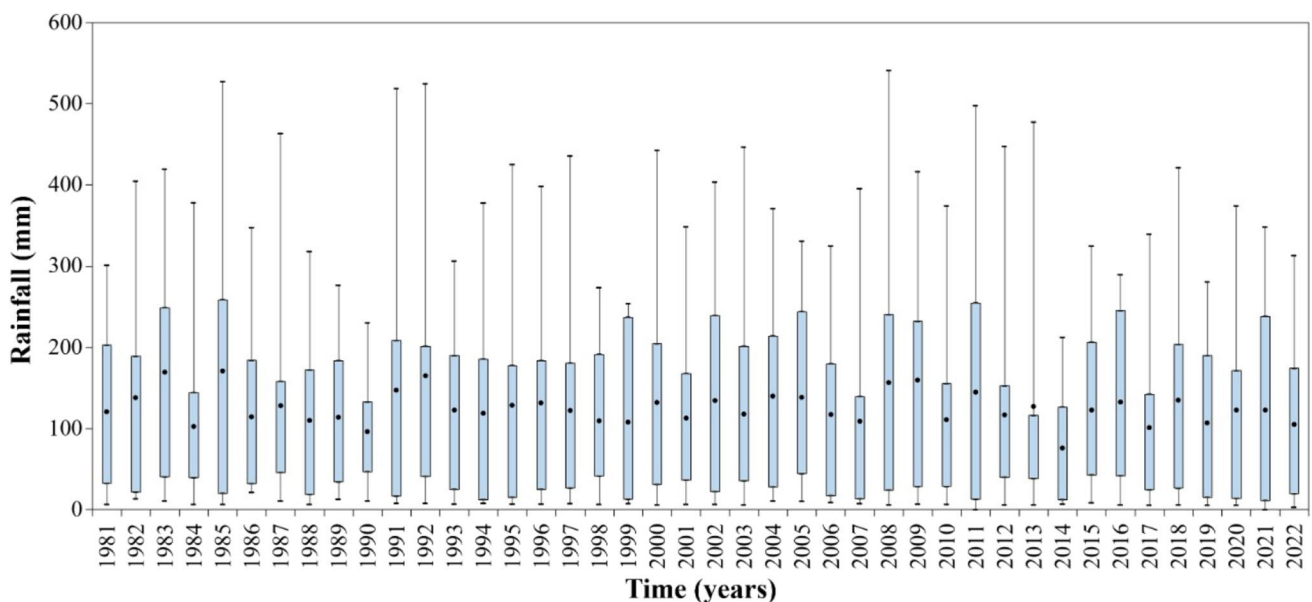


Fig. 2 A box and whisker plot for annual rainfall of every year from 1981 to July 2022

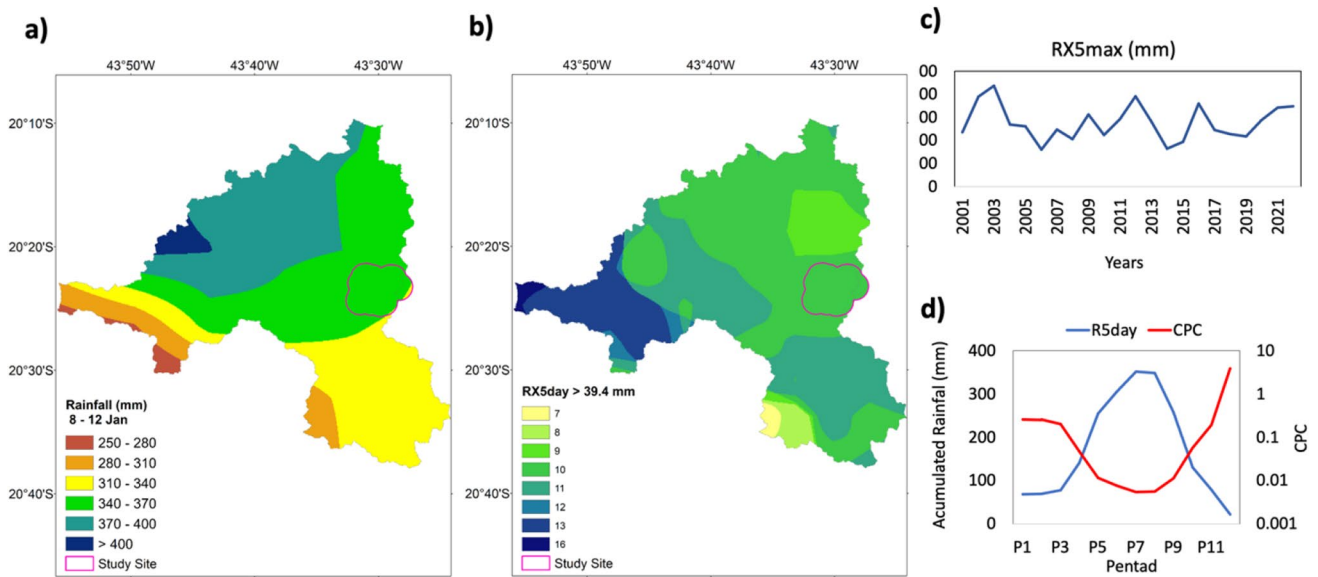


Fig. 3 The accumulated rainfall of 08–12 January in Ouro Preto municipality, southeast Brazil (a), the 5-day accumulated rainfall with value higher than 39.4 mm in January (number of events) (b),

the annual maximum consecutive 5-day precipitation (RX5Max) (c), and the temporal evolution of Rx5Max and the critical precipitation coefficient (CPC) (d)

Table 2 Dickey–Fuller test results for the precipitation time series

Observed value	− 3.466
Critical value	− 3.495
<i>p</i> -value (one-tailed)	0.053
α	0.05

Table 3 Durbin–Watson test results for the precipitation time series

DW	1.841
<i>p</i>	− 0.747
<i>p</i> -value (one-tailed)	0.342
α	0.050

Table 4 Mann–Kendall test results for the precipitation time series

Kendall’s	− 0.087
<i>S'</i>	− 68
Var(<i>S'</i>)	7366.66
<i>p</i> -value (two-tailed)	0.435
α	0.050

The DW test (Table 3) was applied to the precipitation time series to verify the presence of autocorrelation. Autocorrelation refers to the degree of similarity between a given time series and the lagged version of itself over successive time intervals. The DW test showed that the residues of the precipitation time series are not correlated as the *p*-value is greater than the significance level $\alpha = 0.05$. The risk of rejecting the null hypothesis when it is true is less than 3.95%.

The Mann–Kendall test (Table 4) shows that the calculated *p*-value is lower than the significance level $\alpha = 0.05$. Therefore, the null hypothesis cannot be rejected as there is no significant trend in the series. The risk of rejecting the null hypothesis when it is true is less than 3.95%. The continuity correction obtained Sen’s slope equal to 2.185.

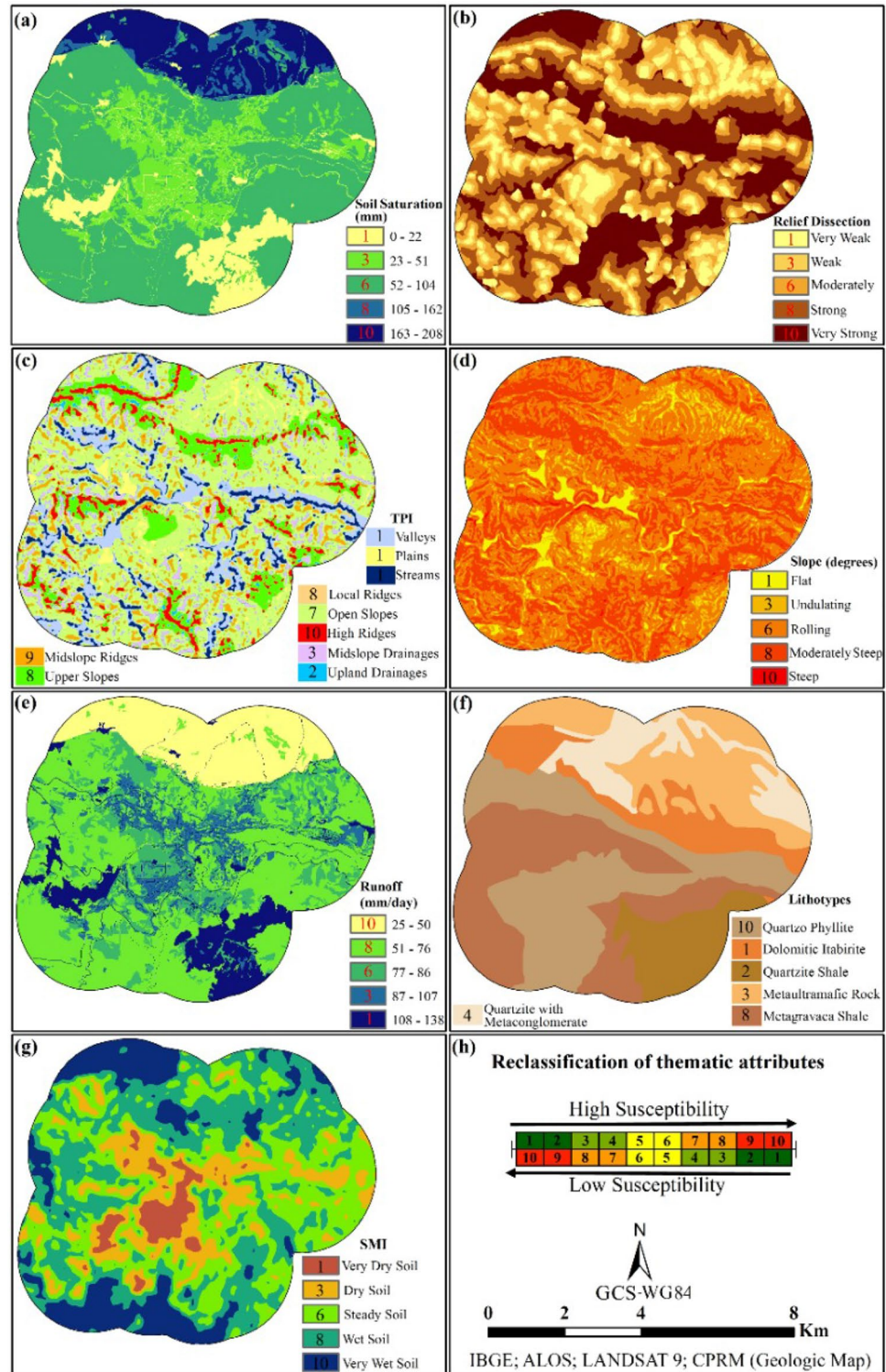
Landslide Susceptibility Map

The landslide susceptibility map was based on the combination of seven thematic maps (Fig. 4): saturation (a); dissection (b); TPI (c); slope (d); curve number (e); geology (f); and SMI (g). Most of Ouro Preto urban areas had a soil saturation of 52–104 mm, relief dissection from very weak to moderate, open and rolling slopes, a quartzose-related geomorphology, runoff from 51 to 76 mm/day, and steady to wet soils (Fig. 4).

The susceptibility map was developed in the two stages of treatment and processing of geographic information. The theoretical phase is based on the reclassification of thematic attributes contained in each map and proposed in the model, using an increasing scale of (dimensionless) values ranging from 1 (least susceptible) to 10 (most susceptible) for each variable (Fig. 4h).

Thus, the second phase (operational) involved the application of the AHP method based on Saaty and Vargas’ scale (1991). The thematic maps were ranked according to their importance for the susceptibility aspect of

Fig. 4 This figure shows the spatial distribution of variables used in the application of the AHP method to map the susceptibility of landslides in Ouro Preto urban areas, southeast Brazil. The following variables were used: (a) soil saturation, (b) relief dissection, (c) topographic position index (TPI), (d) slope, (e) runoff, (f) lithotypes, (g) soil moisture index (SMI), and (h) reclassification of thematic attributes from high to low susceptibility



the analyzed process and compared with each other in a matrix attributing a value of relative importance to the interrelationship of the thematic variables. Therefore, a pairwise comparison matrix was made, where the factors are compared two by two (Table 5).

From these relative values, the weights of the factors (matrix eigenvalue) and the consistency of the matrix judgment (maximum matrix eigenvalue) were calculated. The consistency index (IC) is given by Eq. 5:

Table 5 Pairwise comparison matrix

Factors	Runoff	SMI	TPI	Geology	Slope	Dissection	Saturation
Runoff	1	1/2	1/3	1/5	1/6	1/7	1/9
SMI	2	1	1/1	1/3	1/5	1/6	1/7
TPI	3	2	1	1/2	1/3	1/5	1/6
Geology	5	3	2	1	1/2	1/3	1/5
Slope	6	5	3	2	1	1/2	1/3
Dissection	7	6	5	3	2	1	1/2
Saturation	9	7	6	5	3	2	1

$$IC = \frac{\lambda_{\max} - n}{n - 1} \quad (5)$$

Here, n is the order of the matrix equal to 7, and λ_{\max} is the largest associated eigenvalue equal to 7.1778.

To calculate the consistency ratio (CR), the IC and the random index (RI) are considered, which vary according to the number of variables used in the matrix (n). In this study, the number of variables is seven ($n=7$), obtaining the RI for this number of variables equal to 1.32 (SAATY, 1991). The CR is given by Eq. 6:

$$CR = \frac{IC}{RI} \quad (6)$$

Here, the IC obtained is equal to 0.0296, and the RI given by the literature is equal to 1.32.

As a rule, if the CR is less than 0.1, there is a consistency in proceeding with the AHP calculations. Otherwise, if the CR is higher than 0.1, it is recommended that the judgments be redone until the consistency is adequate (Saaty and Vargas 1991). A CR value of 0.0224 was obtained. Thus, as the CR value is less than 0.1, the values obtained for the proposed model are acceptable, according to the proposed methodology (Saaty and Vargas 1991).

In the judgment of values of relative importance, the saturation map obtained the highest degree of importance over the other variables, followed by the dissection, slope, geology, TPI, and SMI maps. The least important map regarding landslides was the runoff map. This hierarchy was built through empirical observations and integrated analysis of the physical-geographic aspects of this area, in addition to the series of treatments and simulations of the data used in the research (Mantovani and Bacani 2018).

The judgment of these factors compared with each other and adjusted according to the specific characteristics of the region sought to represent the physical conditions found in the study area accurately and reliably. Therefore, when a factor is compared with itself, the only result is 1 as it has equal importance, which is represented on the diagonal of the matrix. This limit is important for the research because, from the moment when all factors intersect, the upper

submatrix becomes a mirror or inverses the values below the lower diagonal (Mantovani and Bacani 2018).

From the values of relative importance of the factors assigned to the matrix variables, the statistical weights for each variable are determined. Each element of the matrix is divided by the sum of the elements of the column to which it belongs, and the average between columns is calculated. Thus, each weight is determined. With the calculated weights and the CR, Eq. 6 was elaborated for the mathematical modeling of the susceptibility to landslides.

$$\begin{aligned} LDE = & 0.3713 \times SAT + 0.2429 \times DIS + 0.1585 \times TPI \\ & + 0.0995 \times SPE + 0.0610 \times RUN + 0.0398 \\ & \times GEO + 0.0264 \times SMI \end{aligned} \quad (7)$$

where LDE is the landslide, SAT is the saturation, DIS is the dissection, TPI is the topographic position index, SPE is the slope, RUN is the runoff, GEO is the geology, and SMI is the soil moisture index.

The map of susceptibility to landslides was generated by applying Eq. 6 in the ArcGIS software with the help of the Raster Calculator tool. Finally, the values obtained by the susceptibility map (1 to 10) were stratified into five classes: very low, low, moderate, high, and very high. Next, in Fig. 5, the susceptibility map in the studied area is presented, and Fig. 6 shows the crossing of the susceptibility classes by the samples of mapped landslides.

Landslide susceptibility map showed that moderate susceptibility represented approximately 31.04% of the total area, with about 18 km²; very low and low susceptibility accounted for approximately 39.65% of the total area, with 23 km² of spatial coverage, while high and very high susceptibility represented together 29.31%, with an area of 17 km².

We found that landslide occurrences were distributed in the most susceptible areas (64% were high and very high: Fig. 6), i.e., 113 occurrences in the “high” class and 79 occurrences in the “very high” class. No occurrence was verified in very low susceptibility sites (Fig. 6).

The areas most affected by very high landslides were rocky outcrops, pasture, and medium- and low-density vegetation (Fig. 7). However, pasture and medium-density vegetation were classified as very low and low susceptibility,

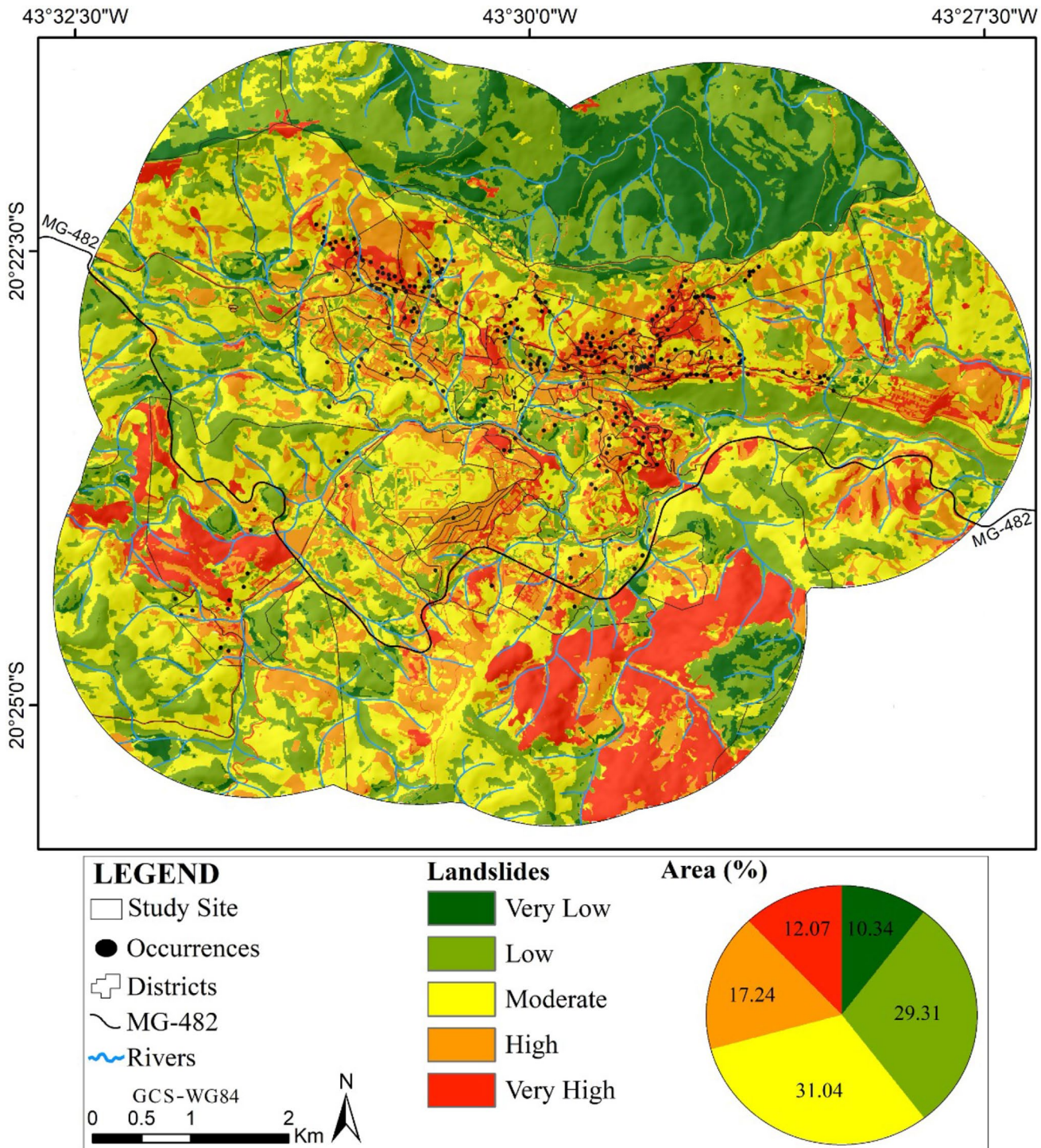


Fig. 5 Landslide susceptibility map in Ouro Preto urban areas, southeast Brazil. The map shows the landslide occurrences superimposed on the susceptibility classification. The susceptibility map was clas-

sified from very low to very high. The figure also shows the area (%) for each landslide class in the study area

respectively, while low-density and rocky outcrops were high and very high susceptibility. Thus, pasture and vegetation sites also need management attention from local governments in hilly areas, despite being classified as

low-susceptibility sites. Among very high-susceptibility classes, rocky outcrops, urban areas, roads, open areas, and mining sites had the largest landslide occurrence (Fig. 7). The largest areas susceptible to landslides are categorized as

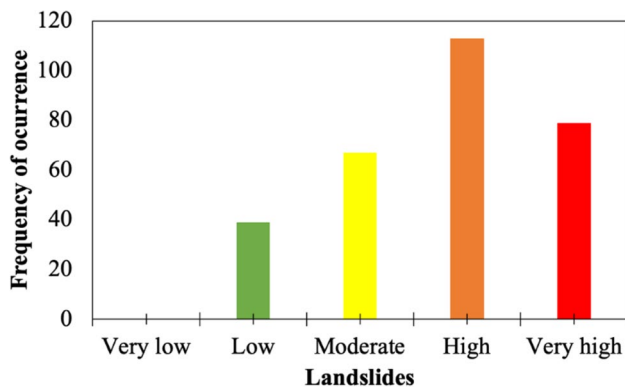


Fig. 6 Susceptibility class (from very low to very high) against frequency of landslide occurrences in Ouro Preto urban areas, southeast Brazil

urban land use areas totaling 33.31 ha (which corresponded to high and very high susceptibility classes: Fig. 7).

Mass movement occurrences with very low kernel density had the greatest spatial coverage of 79.31% of the total area, covering 46 km² with only four occurrences (Fig. 8). This is followed by the “low” class with 6 km² and 43 occurrences of landslides, representing 14.4% of the total landslides. The “moderate” class was the third class in the area with 3 km² and 66 occurrences. The “high” class has 2 km² and a total of 107 occurrences—35% of the total occurrences. The “very high” class has 1 km² and 78 occurrences. Moderate, high, and very high classes overlapped with most landslide occurrences (Fig. 8) and add up to 251 occurrences, accounting for more than 84% of occurrences in the entire study area. This shows that the study area is highly susceptible to landslides as they are mostly concentrated in urbanized areas.

Fig. 7 Landslide occurrence area (hectares) in each land use and land cover (LULC) classification in Ouro Preto urban areas, southeast Brazil, according to landslide susceptibility map classification

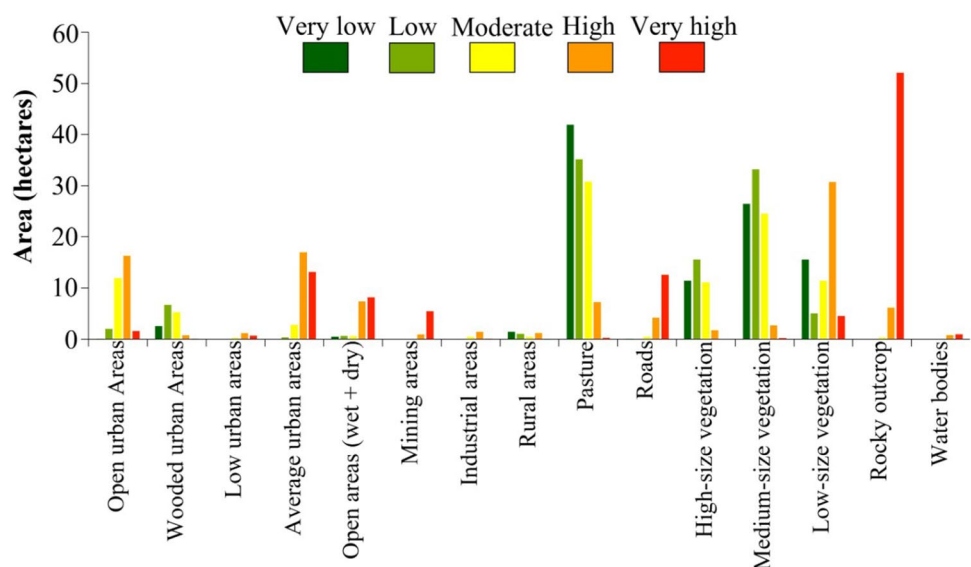
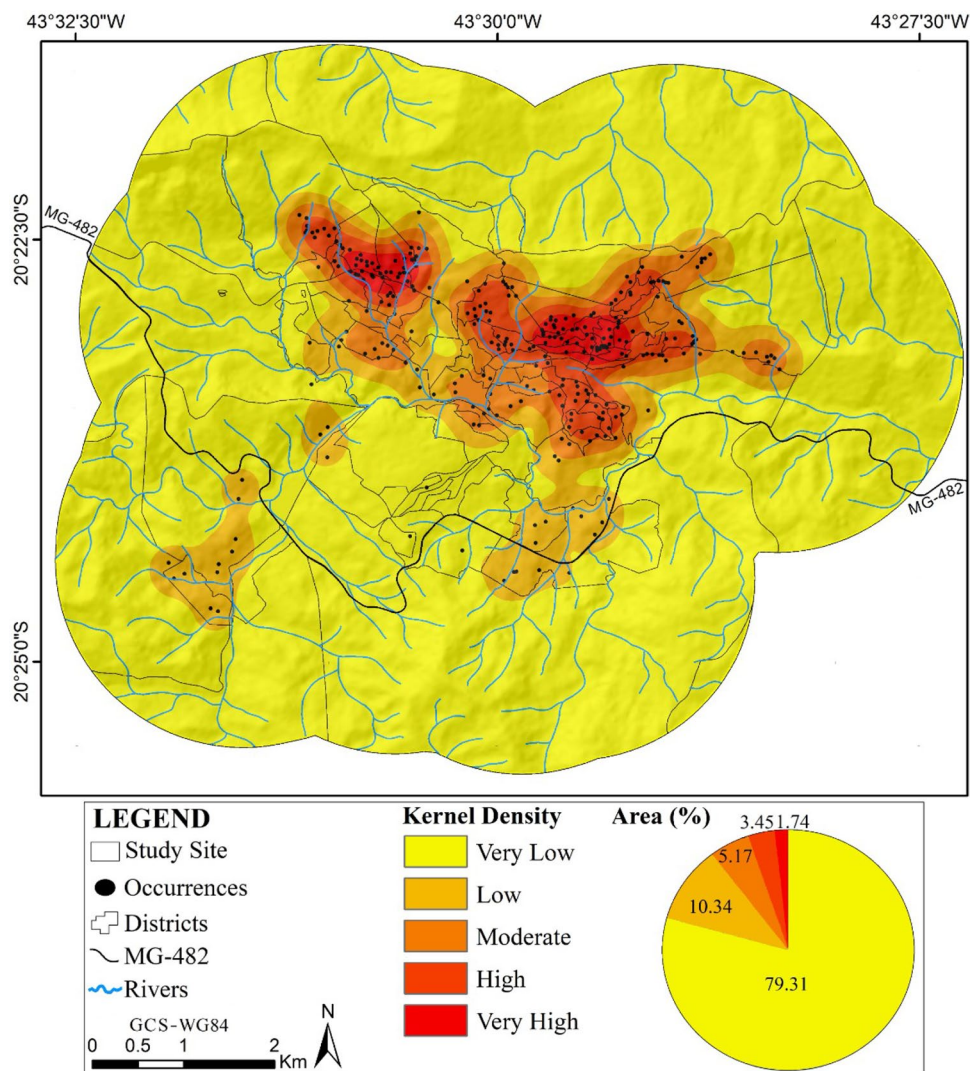


Figure 9 shows photographs of mass movement occurrences located in the study area. The first location is the Antônio Dias neighborhood, Rua Padre Antônio G. Carvalho/Beco Canastra, with high susceptibility to landslides. According to data from the Civil Defense and the Brazilian Geological Survey (CPRM), this neighborhood is a hillside area with a high slope and relief amplitude approximating 30 m (Fig. 9a), comprising soil and rock with foliation triggering landslides. Houses were also developed in a disorderly manner, with buildings characterized as low standard and medium vulnerability. As a result, houses are particularly vulnerable to landslides, leading to high material damage and loss of life. There is a history of small landslides, which occurred between the 1970s and 1980s (CPRM 2006).

The second place in the photograph (Fig. 9b) is in the Padre Faria and Alto da Cruz neighborhoods, Rua Santa Rita and Rua Maciel, with a high risk of landslides. According to the Civil Defense and the CPRM, this area has a steep slope located in a valley with strong fluvial incisions. There is a line of buildings on the crest of this slope. The slope is formed by soil sitting on itabirite, which disrupts the stability of the buildings. In certain places, there are landfills and sloping trees. The proximity of the houses to the slope, combined with the topographical, geological, and geotechnical characteristics of the terrain, contributes to landslides affecting the houses during rainy periods (CPRM 2006).

The third place in the photograph (Fig. 9c) is in Morro da Forca in the central region, where the landslide of January 13, 2022, occurred, destroying two colonial houses. The thinness of the soil and abrupt contact with the rock are factors that trigger landslides. The three occurrences took place in the areas classified by the proposed

Fig. 8 Kernel density map of mass movement occurrences in Ouro Preto urban areas, southeast Brazil. This figure shows the landslide occurrences superimposed on the Kernel density and the area (%) for each Kernel density



methodology as being of “high” and “very high” susceptibility to landslides; consequently, all of them present a risk.

Landslide Mapping Assessment

Using the Boolean Intersection method, we compared the civil defense data and AHP model results for landslides to obtain the areas where landslides were mapped with the AHP classification. The Boolean map highlights the intersection between Figs. 5 and 8. The areas classified as true, that is, areas where there is correspondence between the reference data and the AHP model (Fig. 10). The total area of landslides from civil defense mapping is 0.5575 km² and from AHP was 0.5544 km²; with a difference of 0.55%. The AHP slight underestimation of landslide susceptibility is likely due to the exclusion of landslide class of very small susceptibility.

Discussion

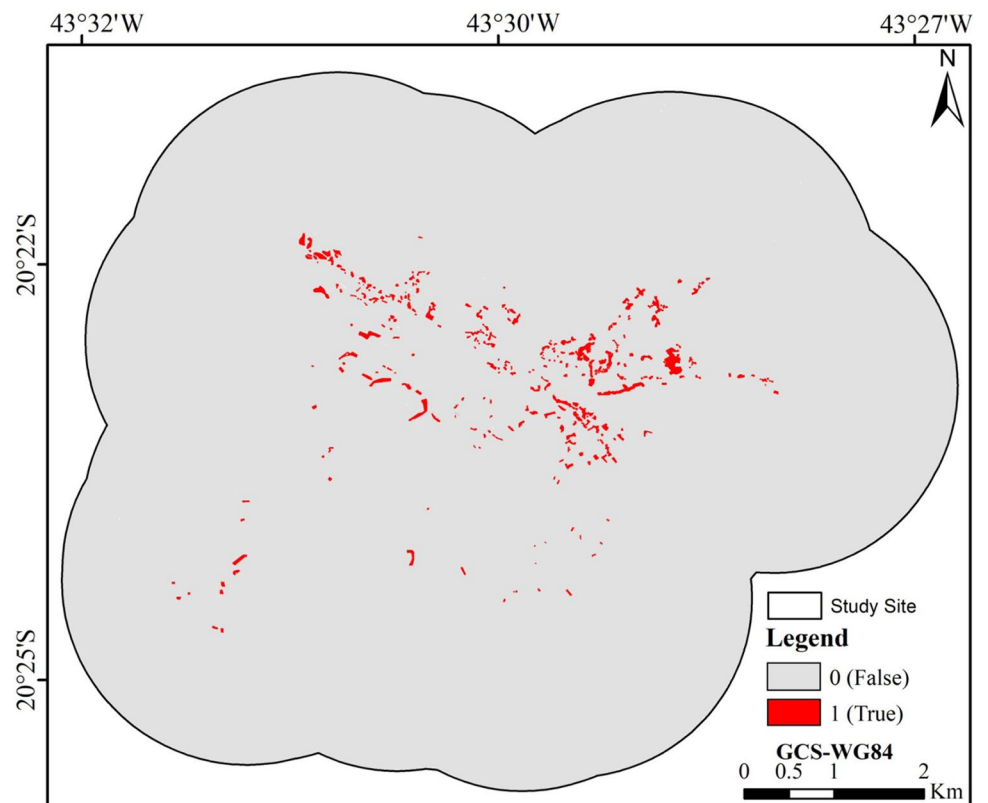
In this paper, we aimed to map and discuss the susceptibility to landslides in the urban area of Ouro Preto, Minas Gerais state, southeast Brazil. Ouro Preto is one of the most vulnerable cities to recurrent landslides in Brazil, resulting in considerable human and economic losses. We found that most of the urban area is moderately susceptible to landslides. Despite that, actual mass movements occurred and have been occurring in moderate, high, and very high classes, especially if under rocky outcrops, urban areas, roads, open areas, and mining sites. We also provided a susceptibility map that could be an important tool for local government and decision-makers.

The analysis of the rainfall time series showed high seasonality. However, there seems to be no tendency for changes in rainfall over the years as it does not have

Fig. 9 Photos of landslides in Ouro Preto, southeast Brazil. Source: Civil Defense of Ouro Preto; CPRM. **a–c** Left and right represent two angles of the same landslide



Fig. 10 Boolean intersection map between civil defense data and the AHP model mapping for landslide occurrence



correlated residues. This shows that there was no extreme event of rainfall on the day of occurrence in 2022, indicating that landslides in Ouro Preto might be associated to rainfall to a small extent, but more likely related to the geographical nature of the houses in urban and municipality area.

Castro (2006) studied rainfall in Ouro Preto from 1988 to 2004 with 417 rainfall episodes. Critical areas were mapped and classified into high, medium, and low risk. Castro found that accumulated rainfall over 5 days was considered the most effective to trigger landslides, where accumulated precipitation of 22 mm/5 days can induce landslides. Precipitation of 124 mm/5 days consequently had a higher risk of landslide occurrences. Nevertheless, this threshold varies among regions based on soil saturation.

In our study, most of the landslide's occurrences took place in the urban areas with rugged relief. For the verified landslides to occur in the urban area, there should be a combination of natural susceptibility with the form of occupation, which determines the risk condition. We found that in the central region of the study area, where the urban area is located, was of particular high risk, as impermeabilization is high, which favors surface runoff and disfavors infiltration and soil moisture. Moreover, Ouro Preto has several landforms with strong slopes and high mountains associated with undulating and strongly undulating reliefs composed mostly of phyllites, and shales. These characteristics justify the area's high susceptibility to landslides. Anthropogenic factors, such as deforestation and urban sprawl, generate instability on hillslopes and induce landslide processes, which sometimes culminate in catastrophic effects (Ávila et al. 2021).

Across the study extent, the southeast region is the most susceptible to landslides because of its physiographic characteristics, such as high slope, high and very high dissection, and the relief of high mountains. It has low infiltration capacity and consequently high surface runoff. Quartzites predominate in the area, and they normally generate more porous, permeable, and humid soils. Together with shales, quartzites increase the potential for landslides. This region is outside the most urbanized area located in the center of the study area; therefore, it is a low-risk region. The second area with the highest susceptibility is southwest of the study area. It also has high slopes and moderate and strong dissection, mainly comprising open slopes and favoring soil moisture. The area has high surface runoff, and its susceptibility is mainly influenced by the lithology of shales and phyllites, which are highly susceptible to landslides. The advantage of this area is that it is not considerably urbanized, resulting in low risk of landslides.

The areas with the lowest susceptibility to landslides and hazards are located north of the study area, mainly to the northeast. They are areas with the highest soil saturation and, consequently, low surface runoff and soil moisture,

which increase its potential for landslides. However, the dissection is mostly weak, with areas of flat and slightly undulating relief formed by meta-ultramafic rocks, quartzites with meta-conglomerate, and itabirites that favor a stable relief in terms of triggering landslides.

Landslides that occurred in 2022 in the region were related to intense soil saturation, with an average monthly rainfall of 122.60 mm in February. This condition associated with the uneven relief and the edaphoclimatic characteristics caused percolation of the surface runoff under the uneven relief, where soil moisture increases in a short period naturally triggered landslide. The magnitude and frequency of landslides are explained by the intensity and distribution of rainfall, the rate of water infiltration into the soil, the degree of soil saturation, and the morphometric and morphological characteristics. However, cutting and filling of land, implementation of constructions without technical monitoring, and urban expansion in irregular areas are considered the main determinants of increased risk in the area. Inadequate management of natural resources, both in urban and rural areas, has been the primary cause of degradation.

Although landslides are natural phenomena, they are often aggravated by population growth and the exploitation of natural resources. This is the case for Ouro Preto, a heritage municipality which was established since 1698, with many preserved buildings and urban configuration. Recent events suggest that the municipality is still focusing on managing post-impact consequences rather than taking actions for disaster risk reduction. Studies mapping landslide susceptibility, as this one, offer an important tool for local government and decision-makers to increase predictions of natural hazard events (Barella et al. 2019) and adopt effective preventive actions.

Conclusion

A novel mathematical model based on multi-criteria decision-making (MCDA) and the Analytic Hierarchy Process (AHP) was used to map the susceptible areas to landslides. Results show that areas most affected by strong landslides were low-density vegetation (high susceptibility) and rocky outcrops (very high susceptibility). Rocky outcrop was the class with the highest landslide occurrence. The susceptibility to landslides map showed that approximately 31.04% of the total area can be classified as moderate susceptibility and 29.31% as high and very high susceptibility. High frequency of landslide occurrence was observed for areas classified with high susceptibility.

The largest areas susceptible to landslides are urban land use areas. Most of the landslide occurrences took place in the urban area with rugged relief because of irregular and unplanned urbanization. Urban areas near rocky outcrops

are more susceptible and can result in human and economic loss; therefore, public policies are needed to prevent future disasters. Landslides that occurred in February 2022 in the region were related to intense soil saturation. With an average monthly rainfall of 122.60 mm, the uneven relief and edaphoclimatic characteristics had caused percolation of the surface runoff, naturally triggering landslides. With a threshold of 39.4 mm (5-day rainfall accumulation) for landslide occurrence, the results showed that only in January 2022, 11 periods of 5-day were above this limit, making the city of Ouro Preto prone to mass movement. This study supports mitigation efforts by local governments and decision-makers.

Declarations

Ethics Approval Not applicable. This research does not involve human participants and/or animal.

Informed Consent Not applicable.

Conflict of Interest The authors declare no conflict of interest.

References

- Alcântara E, Marengo JA, Mantovani J, Londe LR, San RLY, Park E, Lin YN, Wang J, Mendes T, Cunha AP, Pampuch L, Seluchi M, Simões S, Cuartas LA, Goncalves D, Massi K, Alvalá R, Moraes O, Filho CS, Mendes R, Nobre C (2023) Deadly disasters in southeastern South America: flash floods and landslides of February 2022 in Petrópolis, Rio de Janeiro. *Nat Hazards Earth Syst Sci* 23:1157–1175. <https://doi.org/10.5194/nhess-23-1157-2023>
- Amrutha K, Danumah JH, Nikhil S et al (2022) Demarcation of forest fire risk zones in Silent Valley National Park and the effectiveness of forest management regime. *J Geovis Spat Anal* 6:8. <https://doi.org/10.1007/s41651-022-00103-3>
- Ávila FF, Alvalá RC, Mendes RM et al (2021) The influence of land use/land cover variability and rainfall intensity in triggering landslides: a back-analysis study via physically based models. *Nat Hazards* 105:1139–1161. <https://doi.org/10.1007/s11069-020-04324-x>
- Bahrami Y, Hassani H, Maghsoudi A (2021) Landslide susceptibility mapping using AHP and fuzzy methods in the Gilan province. *Iran Geojournal* 86:1797–1816. <https://doi.org/10.1007/s10708-020-10162-y>
- Barella CF, Sobreira FG, Zêzere JL (2019) A comparative analysis of statistical landslide susceptibility mapping in the southeast region of Minas Gerais state, Brazil. *Bull Eng Geol Environ* 78:3205–3221. <https://doi.org/10.1007/s10064-018-1341-3>
- Carvalho Filho A, Curi N, Shinzato E (2010) Relações solo-paisagem no Quadrilátero Ferrífero em Minas Gerais. *Pesquisa. Agropecuária Bras* 903-916. <https://doi.org/10.1590/S0100-204X2010000800017>
- Castro JMG (2006) Pluviosidade e movimentos de massa nas encostas de Ouro Preto. 138 f. Dissertação (Mestrado em Ciências da Engenharia Civil) - Universidade Federal de Ouro Preto. Available: <http://www.repositorio.ufop.br/jspui/handle/123456789/2737>
- COMPANHIA DE PESQUISA DE RECURSOS MINERAIS - CPRM (2006) Mapa Geodiversidade do Brasil: Influência da geologia dos grandes geossistemas no uso e ocupação dos terrenos. Brasília: CPRM, p 68. Available: <http://www.cprm.gov.br/publique/Gestao-Territorial/Gestao-Territorial/Mapas-de-Geodiversidade-Estaduais-1339.html>
- Domínguez-Cuesta MJ (2013) Susceptibility. In: Bobrowsky, P.T. (eds) *Encyclopedia of natural hazards*. Encyclopedia of earth sciences series. Springer, Dordrecht. https://doi.org/10.1007/978-1-4020-4399-4_340
- Durbin JWGS (1950) Testing for serial correlation in least squares regression. I *Biometrika* 37(3–4):409–428. <https://doi.org/10.1093/biomet/37.3-4.409>. JSTOR2332391
- Durbin JWGS (1951) Testing for serial correlation in least squares regression. II *Biometrika* 38(1–2):159–179. <https://doi.org/10.1093/biomet/38.1-2.159>. JSTOR2332325
- EMPRESA BRASILEIRA DE PESQUISA AGROPECUÁRIA - EMBRAPA (2018) Sistema Brasileiro de Classificação de Solos. 5 ed. Rio de Janeiro: Embrapa Solos, p 353. Available: <https://www.infoteca.cnptia.embrapa.br/handle/doc/1094003>
- Fernandes NF, Amaral CP (1996) *Geomorfologia e Meio Ambiente*. Bertrand Brasil, Rio de Janeiro, pp 123–194p
- Fuller WA (1996) *Introduction to statistical time series*. 2nd edn., Wiley
- Funk C, Peterson P, Landsfeld M et al (2015) The climate hazards infrared precipitation with stations—a new environmental record for monitoring extremes. *Sci Data* 2:150066. <https://doi.org/10.1038/sdata.2015.66>
- Guimarães FS, Cordeiro CM, Bueno GT, Carvalho VLM, Nero MA (2017) Uma proposta para automatização do Índice de dissecação do relevo. *Revista Brasileira de Geomorfologia*, São Paulo 18(1):155–167. <https://doi.org/10.20502/rbg.v18i1.1163>
- Guisan A, Weiss SB, Weiss AD (1999) GLM versus CCA spatial modeling of plant species distribution. *Kluwer Academic Publishers. Plant Ecol* 143:107–122. <https://doi.org/10.1023/A:1009841519580>
- Hassan MK, Abbas BA, Garas SN (2019) Readability, governance, and performance: a test of the obfuscation hypothesis in Qatari listed firms. *Corp Gov: Int J Bus Soc* 19(2):270–298. <https://doi.org/10.1108/CG05-2018-0182>
- INSTITUTO BRASILEIRO DE GEOGRAFIA E ESTATÍSTICA - IBGE (1991) *Classificação da vegetação brasileira adaptada a um sistema universal*. IBGE, Rio de Janeiro
- IPCC, Climate Change (2022) *Impacts, adaptation, and vulnerability. Contribution of Working Group II to the Sixth Assessment Report of the Intergovernmental Panel on Climate Change* [H.-O. Pörtner DC, Roberts M, Tignor ES, Poloczanska K, Mintenbeck A, Alegría M, Craig S, Langsdorf S, Löschke V, Möller A, Okem B, Rama (eds.)]. Cambridge University Press. Available: <https://www.ipcc.ch/report/sixth-assessment-report-working-group-ii/>
- Kalsnes B, Capobianco V (2022) Use of vegetation for landslide risk mitigation. In: et al. *Climate adaptation modelling*. Springer Climate. Springer, Cham. https://doi.org/10.1007/978-3-030-86211-4_10
- Leonardi G, Palamara R, Manti F, Tufano A (2022) GIS-multicriteria analysis using AHP to evaluate the landslide risk in road lifelines. *Appl Sci* 12:4707. <https://doi.org/10.3390/app12094707>
- Mantovani JR, Bacani VM (2018) Uma proposta metodológica de mapeamento de áreas suscetíveis a inundação e/ou alagamento na bacia hidrográfica do córrego Indaiá-MS. *Geosp – Espaço e Tempo (Online)*, 22(3), p. 687-706. ISSN 2179-0892
- Mantovani JR, Bueno GT (2021) Uma proposta metodológica para mapear a dissecação do relevo e aplicá-la no Parque Nacional da Serra da Canastra-MG. *Geosp* 25(1):1–19 (e-170745. ISSN 2179-0892)

- Mantovani JR, Sakamoto AY, Gradella FS, Braz AM (2017) Análise do comportamento do NDWI sob diferentes intensidades da pluviosidade no Pantanal da Nhecolândia, MS-Brasil. Anais do XVIII Simpósio Brasileiro de Sensoriamento Remoto. Anais eletrônicos. Santos
- Medeiros LC, Ferreira N, Ferreira LG (2009) Avaliação de modelos digitais de elevação para delimitação automática de bacias hidrográficas. Revista Brasileira de Cartografia, n. 61/2. Available:<https://seer.ufu.br/index.php/revistabrasileiracartografia/article/view/44844>
- Melesse AM, Shih SF (2002) Spatially distributed storm runoff depth estimation using Landsat images and GIS. Comput Electron Agric 37(1–3):173–183. [https://doi.org/10.1016/S0168-1699\(02\)00111-4](https://doi.org/10.1016/S0168-1699(02)00111-4)
- Mersha T, Meten M (2020) GIS-based landslide susceptibility mapping and assessment using bivariate statistical methods in Simada area, northwestern Ethiopia. Geoenviron Disasters 7:20. <https://doi.org/10.1186/s40677-020-00155-x>
- NATURAL RESOURCES CONSERVATION SERVICE - NRCS (2009) Chapter 7: Hydrologic soil groups. In: National engineering handbook: Part 630, Hydrology. Available: <http://directives.sc.egov.usda.gov/>
- Nikhil S, Danumah JH, Saha S et al (2021) Application of GIS and AHP method in forest fire risk zone mapping: a study of the Parambikulam Tiger Reserve, Kerala, India J Geovis Spat Anal 5:14. <https://doi.org/10.1007/s41651-021-00082-x>
- Oliveira MAS, Brito SN (1998) A. in Geologia de Engenharia. São Paulo: Associação Brasileira de Geologia de Engenharia
- Quevedo RP, Velastegui-Montoya A, Montalván-Burbano N et al (2023) Land use and land cover as a conditioning factor in landslide susceptibility: a literature review. Landslides. <https://doi.org/10.1007/s10346-022-02020-4>
- Rozante J, Moreira DS, Goncalves LG, Vila D (2010) Combining TRMM and surface observations of precipitation: technique and validation over South America. Weather Forecast 25. <https://doi.org/10.1175/2010WAF2222325.1>
- Saaty TL (1977) A scaling method for priorities in hierarchical structures. J Math Psychol 15(3):234–281
- Saaty TL, Vargas LG (1991) Prediction: projection and forecasting. Kluwer Academic, Boston
- Sartori A, Genovez AM, Lombardi Neto F (2011) Classificação hidrológica de solos brasileiros para a estimativa de chuva excedente com o método do serviço de conservação do solo dos Estados Unidos – Parte 1: Classificação. Revista Brasileira De Recursos Hídricos 10:5–18
- Sen PK (1968) Estimates of the regression coefficient based on Kendall's Tau. J Am Statist Assoc 63:1379–1389. <https://doi.org/10.1080/01621459.1968.10480934>
- Shano L, Raghuvansh TK, Meten M (2020) Landslide susceptibility evaluation and hazard zonation techniques – a review. Geoenviron Disasters 7:1–19. <https://doi.org/10.1186/s40677-020-00152-0>
- Shu H, Hürlimann M, Molowny-Horas R, González M, Pinyol J, Abancó C, Ma J (2019) Relation between land cover and landslides susceptibility in Val d' Aran, Pyrenees (Spain): historical aspects, presente situation and forward prediction. Sci Total Environ 693:133557
- Skilodimou HD, Bathrellos GD, Koskeridou E, Soukis K, Rozos D (2018) Physical and anthropogenic factors related to landslide activity in the northern Peloponnese, Greece. Land 7:85. <https://doi.org/10.3390/land7030085>
- Thomas AV, Saha S, Danumah JH et al (2021) Landslide susceptibility zonation of Idukki district using GIS in the aftermath of 2018 Kerala floods and landslides: a comparison of AHP and frequency ratio methods. J Geovis Spat Anal 5:21. <https://doi.org/10.1007/s41651-021-00090-x>
- Tominaga LK, Santoro J, Amaral R (2009) Desastres Naturais: conhecer para prevenir. São Paulo: Instituto Geológico, Secretaria de Meio Ambiente. 197 p ISBN 978-85-87235-09-1
- Wang L, Liu H (2006) An efficient method for identifying and filling surface depressions in digital elevation models for hydrologic analysis and modelling. Int J Geogr Inf Sci 20:193–213. <https://doi.org/10.1080/13658810500433453>
- Zeng Y, Feng Z, Xiang N (2004) Assessment of soil moisture using Landsat ETM+ temperature/vegetation index in semiarid environment. IEEE Trans Geosci Remote Sens 6:4036–4039
- Zimmerman BJ (1998) Developing self-fulfilling cycles of academic regulation: an analysis of exemplary instructional models. In: Schunk DH, e Zimmerman BJ (eds.) Self-regulated learning: from teaching to self-reflective practice. Nova York, The Guilford Press, pp 1–19
- Publisher's Note** Springer Nature remains neutral with regard to jurisdictional claims in published maps and institutional affiliations.
- Springer Nature or its licensor (e.g. a society or other partner) holds exclusive rights to this article under a publishing agreement with the author(s) or other rightsholder(s); author self-archiving of the accepted manuscript version of this article is solely governed by the terms of such publishing agreement and applicable law.